

Dynamical condensation in a magnetized and thermally bistable flow

Application to interstellar cirrus

P. Hennebelle and M. Pérault

Laboratoire de radioastronomie millimétrique, UMR 8540 du CNRS, École normale supérieure et Observatoire de Paris, 24 rue Lhomond, 75231 Paris cedex 05, France

Received 23 December 1999 / Accepted 22 May 2000

Abstract. We investigate the dynamical condensation process in a magnetized and thermally bistable flow, in one dimensional (slab) geometry. We find self-similar solutions able to describe the magneto-thermal process for weakly heterogeneous magnetic fields and perform a numerical simulation in the general case corresponding to the neutral interstellar medium. It is well known that a purely transverse magnetic field can prevent the condensation because magnetic pressure increases with density. In a converging flow however, if the field is oblique, the magnetic field lines are compressed and bent. The fluid is driven forward ahead of the original compression. The magnetic tension induces transverse velocities which tend to unbend the field lines. Two cases arise: in weak fields the transverse flow aligns the field lines parallel to the initial flow close to the convergence center, leading to an unimpeded central condensation along this direction. Stronger fields rapidly re-align the flow in the field direction, leading to condensation along the original field direction. The conditions for condensation are similar to the non magnetized case, with the additional constraint of a maximum angle between the initial fields. This constraint is most severe when kinetic and magnetic energies are comparable.

At the end of the condensation, the magnetic field slowly relaxes back to its original direction, resulting in fields of identical intensity in the cloud and in the intercloud gas. For the neutral atomic interstellar medium, the maximum angle is in the range 20 to 40 degrees.

Key words: magnetic fields – Magnetohydrodynamics (MHD) – instabilities – book reviews – ISM: structure – ISM: clouds

1. Introduction

The neutral interstellar medium is usually described as a thermally bistable medium with a warm and diffuse phase (warm neutral medium, WNM) and a cold and dense phase (cold neutral medium, CNM) in rough pressure equilibrium. Field et al. (1969), Bergeron & Souffrin (1971), Wolfire et al. (1995) have made theoretical studies and Kulkarni & Heiles (1987), Dickey

& Lockman (1990), Joncas et al. (1992), Hartmann (1994) observational ones. Measurements of the magnetic interstellar field in the atomic gas (HI) at scales below 100 pc (Heiles 1987, Troland & Heiles 1986, Myers et al. 1995) give values around $5 \mu\text{G}$ with evidence for a small ordered component and a random one. They show that the magnetic intensity is on average independent of the density in the range 0.1 to 100 cm^{-3} , i.e. the WNM and the CNM roughly have the same magnetic field. In both cases, thermal and magnetic energies have comparable orders of magnitude. Troland & Heiles (1986) argue that the concept of “relatively quiescent streaming of low-density gas along the field lines” (Parker instability at the $\simeq 1$ kpc scale), which would naturally account for relatively constant field strengths, contradicts the evidence for supersonic flows. A theory of the formation of small scale CNM structures must account for these facts. For higher densities ρ , the gas is gravitationally bound and the mean value of the magnetic field B increases with density (Crutcher 1999). Mouschovias (1976 a, b) and Scott & Black (1980) derive a theoretical relation between B and ρ , namely:

$$\frac{B}{B_0} = \left(\frac{\rho}{\rho_0} \right)^k,$$

where k takes values between $1/3$ and $1/2$.

Various studies deal with magneto-thermal processes. Field (1965), Oran et al. (1982), and Loewenstein (1990) investigate the effects of magnetic field on thermal instability. Balbus (1986) and Steele & Ibánñez (1999) consider magneto-thermal fronts. David & Bregman (1989) study the thermal instability with magnetic fields in the non-linear regime and note that even magnetic fields as weak as $1 \mu\text{G}$ can prevent the condensation. Friaça & Jafelice (1999) argue that the magnetic field has to be dissipated and consider the problem of magnetic reconnection. Gammie & Ostriker (1996) demonstrate that non-linear magnetic waves lead to strong density contrasts. However, their isothermal assumption is not suited to the study of thermal condensation. Elmegreen (1997) avoids this restriction and introduces more realistic thermal processes. He shows that non-linear magnetic waves in a thermally bistable medium produce a bimodal structure with dense clouds embedded in a diffuse intercloud medium. However, he starts from a uniform, thermally unstable medium that is neither CNM nor WNM, and it

is unclear whether the two phases can exchange matter and how. Large-scale simulations of turbulent magnetized flows, including thermal processes (without thermal instability between 10^2 and 10^4 K), galactic rotation, star formation and gravity, have been performed by Passot et al. (1995) (see also Gazol-Patiño & Passot 1999, Ballesteros-Paredes et al. 1999 and Korpi et al. 1999). They study the role of the magnetic field on cloud formation and conclude, in a very extensive article, that condensations still happen for large magnetic fields (see for example Run 61 of Passot et al. 1995). Very recently Vázquez et al. (2000) investigated the development and the effects of the thermal instability in their simulations of the turbulent galactic gas and Burkert & Lin (2000) considered the emergence of small scale perturbations in a thermally unstable cloud.

Recently, Kovalenko & Shchekinov (1999) considered linear perturbations in a thermally bistable gas, initially near the unstable point ($dP/d\rho = 0$). They demonstrate that thermal condensation occurs and they numerically follow the non-linear evolution. Independently we studied (Hennebelle & Pérault (1999) hereafter paper I) the case of finite-amplitude velocity perturbations in a thermally bistable flow initially at thermal equilibrium in the diffuse phase. The diffuse phase is linearly stable but non-linearly unstable; compression can drive parcels of gas into unstable conditions, where they strongly condense until they reach the other thermal equilibrium branch (CNM). We showed that a thermal condensation occurs if the typical scale of the perturbation is large enough and the peak of the initial velocity field reaches a given threshold. We concluded that the dynamical condensation is much more efficient than the conductive condensation: the structure growth is much faster during a compression than in a quasi-isobaric medium. In a thermally bistable flow, compression effects are very important and cannot be ignored.

In our previous study, we ignored the magnetic field and one can wonder whether the condensation process still happens in the presence of magnetic field. What are the consequences of a magnetic field for thermal condensation? Condensation is always possible along the field lines, but a perfect alignment between magnetic and velocity fields is very unlikely and even a small transverse component can strongly affect the non-linear regime.

In the present article, we analytically and numerically study the dynamical condensation of a magnetized, thermally bistable flow. We deliberately ignore other physical aspects, like gravity or galactic rotation, in order to concentrate on dynamical magneto-thermal processes and restrict ourselves to 1-D slab geometry. Our approach is similar in many ways to the situation considered by Elmegreen (1997). The main difference is that condensation from the stable warm phase is driven by a converging flow rather than by non-linear magnetic waves. Further, we focus on one single event (compression leading to the formation of one cloud) whereas Elmegreen considers a larger scale with several clouds. Our approach aims at a detailed analysis and understanding of the MHD condensation mechanism.

Sect. 2 presents the equations of the problem, the notations, the orders of magnitude, and gives a qualitative discussion of the

problem. Sect. 3 is an analytical investigation of the condensation and focuses on magnetic aspects. We derive self-similar solutions which describe the magneto-thermal process and show how strong condensations are possible in a magnetized gas. Sect. 4 presents a one-dimensional numerical simulation of the thermal condensation in the thermally bistable interstellar gas. Discussion and conclusions are given in Sect. 5.

2. Tension versus magnetic pressure

2.1. Equations and notations

We consider the equations of magneto-hydrodynamics for a perfect gas including thermal exchanges with the surrounding medium (equations of radiative flows). S.I. units are used throughout the paper. Conversion to cgs units is also given for easier reference. These equations are

$$\frac{\partial \rho}{\partial t} + \mathbf{V} \cdot \mathbf{grad} \rho + \rho \operatorname{div} \mathbf{V} = 0, \quad (1)$$

$$\rho \left(\frac{\partial \mathbf{V}}{\partial t} + \mathbf{V} \cdot \mathbf{grad} \mathbf{V} \right) = -\mathbf{grad} P + \frac{1}{\mu_0} \mathbf{rot} \mathbf{B} \wedge \mathbf{B} + \operatorname{div} \overleftrightarrow{\Pi}, \quad (2)$$

$$P = \frac{\rho}{M_p} k_b T, \quad (3)$$

$$C_v \rho \left(\frac{\partial T}{\partial t} + \mathbf{V} \cdot \mathbf{grad} T + (\gamma - 1) T \operatorname{div} \mathbf{V} \right) = -\rho \mathcal{L}(\rho, T) - \operatorname{div} \mathbf{j} + \Pi_{ij} \partial_{x_j} V_i, \quad (4)$$

$$\frac{\partial \mathbf{B}}{\partial t} + \mathbf{V} \cdot \mathbf{grad} \mathbf{B} - \mathbf{B} \cdot \mathbf{grad} \mathbf{V} + \mathbf{B} \operatorname{div} \mathbf{V} = 0. \quad (5)$$

$$\operatorname{div} \mathbf{B} = 0. \quad (6)$$

The drift between ions and neutrals is a small effect in a medium with an ionization fraction around $10^{-3}/10^{-2}$ like the interstellar diffuse neutral gas, and is neglected.

As usual, ρ is the density, T the temperature, P the pressure, \mathbf{V} the velocity and \mathbf{B} the magnetic field. $\overleftrightarrow{\Pi}$ is the viscous stress tensor, $\mathbf{j} = -\kappa(T) \mathbf{grad} T$ the heat flux, κ the thermal conductivity, C_v the heat capacity, M_p the mean particle mass, k_b the Boltzmann constant, μ_0 the magnetic permeability ($4\pi \cdot 10^{-7} \text{ T}^2 \text{ J}^{-1} \text{ m}^3$), γ the adiabatic index, \mathcal{L} the net loss function (cooling minus heating), C_s denotes the sound speed,

$$\tau_{\text{rad}} = C_v T / \langle \mathcal{L} \rangle, \quad \lambda_F = \sqrt{\kappa T / \rho \langle \mathcal{L} \rangle}$$

are respectively the cooling or radiation time and Field length. The viscosity and thermal diffusivity are (Lang 1974)

$$\eta = 5.7 \cdot 10^{-6} \left(\frac{T}{1 \text{ K}} \right) \text{ kg m}^{-1} \text{ s}^{-1}. \quad \kappa = \frac{5}{3} C_v \eta.$$

In a magnetized gas, the thermal diffusivity depends on the magnetic field and is considerably reduced perpendicularly to the field lines (Spitzer 1962, Balbus 1986, Steele & Ibánñez 1999). However, in the dynamical problem considered here, the dissipative terms are small until the quasi-isobaric regime is reached. In the present article, we focus on the dynamical aspects of the condensation process, so we neglect the dependence of thermal diffusivity on magnetic field. Typical values in the WNM are

$$C_s \simeq 10^4 \text{ m s}^{-1}, \tau_{\text{rad}} \simeq 10^{12} \text{ s}, \lambda_F \simeq 0.1 \text{ pc},$$

$$T \simeq 10^4 \text{ K}, P \simeq 10^{-13} \text{ J m}^{-3} (10^{-12} \text{ erg cm}^{-3}),$$

$$\rho/M_p \simeq 0.5 \cdot 10^6 \text{ m}^{-3} (0.5 \text{ cm}^{-3}), B \simeq 5 \cdot 10^{-10} \text{ T} (5 \mu\text{G}).$$

2.2. Thermal condensation in slab geometry with magnetic fields

Let us give a qualitative description of the physical process developed in subsequent sections. Like Elmegreen (1997) and Gammie & Ostriker (1996), we consider the problem in the slab geometry. The transverse fields V_y and B_y are not zero but depend on x only. The longitudinal field B_x is uniform and constant. We consider a converging flow in a thermally bistable medium. We showed in Paper I, that in a non-magnetized gas initially at thermal equilibrium in the WNM phase, if the typical spatial scale is at least equal to $\tau_{\text{rad}} C_s$ and if the velocity peak reaches a critical value, thermal condensation occurs. Part of the gas leaves the first equilibrium branch (WNM) and reaches the second one (CNM). To what extent does the magnetic field alter this picture?

2.2.1. Case of a transverse field

If a purely transverse magnetic component is added, magnetic pressure must be taken into account. From the standard interstellar thermal pressure, a local density enhancement of around 3 is necessary to reach the critical point (Paper I). This enhances the magnetic pressure by a factor 9. For $B = 3 \cdot 10^{-10} \text{ T} (3 \mu\text{G})$, the magnetic pressure reaches a value about three times the initial pressure in the flow. Even with a weak initial field supersonic motions must be considered in order to reach the critical point. The subsequent evolution of the thermally unstable gas is further affected by magnetic pressure and condensation is rapidly stopped. A rough estimate of the final cloud density can be made assuming mechanical equilibrium between the thermally dominated diffuse medium and the magnetically dominated dense medium. With subscript 0 denoting values for the diffuse phase and subscript 1 for the dense one

$$P_{\text{th},0} \simeq P_{\text{mag},1} = \frac{B_1^2}{2\mu_0} = \left(\frac{\rho_1}{\rho_0}\right)^2 \frac{B_0^2}{2\mu_0}, \quad (7)$$

hence,

$$\frac{\rho_1}{\rho_0} \simeq \sqrt{8\pi} \left(\frac{P_{\text{th},0}}{10^{-13} \text{ J m}^{-3}}\right)^{\frac{1}{2}} \left(\frac{10^{-10} \text{ T}}{B_0}\right)^{\frac{1}{2}}. \quad (8)$$

A magnetic field of only $10^{-10} \text{ T} (1 \mu\text{G})$ thus leads to a maximum density ratio of about 5, far from the value derived from observations (Kulkarni & Heiles 1987). For higher values of the magnetic field, only transient weakly contrasted structures can emerge.

2.2.2. Case of an oblique magnetic field

Let ω denote the angle between the magnetic and velocity fields ($\omega = 0$ means that \mathbf{B} and \mathbf{V} are parallel). In such conditions a magnetic tension applies to the flow, and consequently a (heterogeneous) transverse velocity field appears and contributes to the evolution of the magnetic field. In the slab geometry Eq. (5) becomes

$$\partial_t B_y + \partial_x (B_y V_x) = \partial_x (B_x V_y). \quad (9)$$

If B_x is not vanishing, the r.h.s. can be seen as a transport term and $B_x V_y$ as a current of B_y that contributes to the evolution of the transverse magnetic component. For sufficient values of the longitudinal magnetic field, it possibly allows for the magnetic pressure to decrease. More physically, the longitudinal velocity compresses and bends the field lines. Thus, it enhances pressure and magnetic tension. The magnetic tension, on the contrary, tends to unbend these lines and decreases the magnetic pressure.

We can also formulate this process using the flux freezing concept. Let us consider a rectangle A in the plane $y = 0$, delimited by x_0 and x_1 . Let h_0 be its length along the z-axis. The magnetic flux through any surface is conserved

$$\frac{d\Phi}{dt} = \frac{d}{dt} \int_A \mathbf{B} \cdot d\mathbf{S} = 0, \quad (10)$$

at initial time

$$\Phi = h_0 \int_{x_0}^{x_1} B_y(x) dx. \quad (11)$$

If the longitudinal component is equal to zero, then A will always belong to the plane $y = 0$ and if $x_1(t) - x_0(t)$ decreases (compression), B_y increases in order to keep the magnetic flux constant. With a non-vanishing magnetic longitudinal component, the rectangle A is stretched in the y-direction and the expression of the magnetic flux becomes

$$\Phi = h_0 \left(\int_{x_0(t)}^{x_1(t)} B_y(x) dx + B_x \left(\int_0^t v_y(x_1(t')) dt' - \int_0^t v_y(x_0(t')) dt' \right) \right). \quad (12)$$

Eq. (2) gives the evolution of the transverse velocity field, and in slab geometry leads to

$$\frac{\Phi}{h_0} = \int_{x_0(t)}^{x_1(t)} B_y(x) dx + \frac{B_x^2}{\mu_0} \times \int_0^t \int_0^{t'} \left(\frac{\partial_x B_y(x_1(t''))}{\rho(x_1(t''))} - \frac{\partial_x B_y(x_0(t''))}{\rho(x_0(t''))} \right) dt'' dt'. \quad (13)$$

Consequently, if $l(t) = x_1(t) - x_0(t)$ decreases, B_y does not necessarily increase and for sufficient values of B_x the thermal

condensation keeps going on. This is demonstrated analytically in Sect. 3 and numerically in Sect. 4.

3. Self-similar solutions of a magneto-thermal condensation

Self-similar solutions of the idealised (all dissipative terms are neglected) system of Eqs. (1–6) can be obtained, with a slight additional approximation. The system is then reduced to a single ordinary differential equation, derived in Appendix A, and numerically solved in Sects. 3.3, 3.4. Exact solutions for special cases are found in Appendix B and C.

3.1. Reduction to a single ordinary differential equation

Self-similar solutions are widely found in the literature in several contexts (Sedov 1959, Barenblatt & Zeldovich 1972, Ferrara & Shchekinov 1996, Shu 1977, Li & Shu 1997, Munier & Feix 1982, Bouquet et al. 1985). They are known to describe intermediate regimes, that do not depend on the initial and boundary conditions. These exact solutions usually offer a deep insight into the physical processes; they mainly provide an analytical description of fully non-linear processes that cannot be described by linear or weakly non-linear analysis.

Let us consider the idealised system of Eq. (1–6). We first normalize these equations (ρ_0 is the equilibrium gas density in the WNM) and set

$$\tau = t/\tau_{\text{rad}}, \quad \tilde{x} = x/C_s\tau_{\text{rad}}, \quad \tilde{V}_i = V_i/C_s,$$

$$\tilde{\rho} = \rho/\rho_0, \quad \tilde{P} = P/\rho_0 C_s^2, \quad \tilde{T} = T/\frac{M_p C_s^2}{k_b},$$

$$\tilde{\mathcal{L}} = \mathcal{L}/\frac{C_s^2}{(\gamma-1)\tau_{\text{rad}}}, \quad \tilde{B}_i = B_i/\sqrt{\mu_0\rho_0 C_s^2}.$$

We assume that the x-component of the velocity field is

$$\tilde{V}_x = \frac{\dot{a}(\tau)}{a(\tau)} \tilde{x}, \quad (14)$$

where a is a function of τ and \dot{a} its derivative against τ . This field diverges at infinity, but can be relevant locally. The associated density field is

$$\tilde{\rho}(\tau, \tilde{x}) = \frac{1}{a} f\left(\frac{\tilde{x}}{a}\right) = \frac{1}{a} f(x'), \quad (15)$$

where f is an arbitrary function and $x' = \tilde{x}/a(\tau)$. We now consider a magnetic field equal to

$$\tilde{B}_x(x', \tau) = b_1^0, \quad (16)$$

$$\tilde{B}_y(x', \tau) = b_3(\tau) + b_2(\tau) F(x'), \quad (17)$$

where

$$F(x') = \int_0^{x'} f(u) u du, \quad (18)$$

and assume that the magnetic field is only weakly heterogeneous, or

$$b_3 \gg b_2 F(x') \quad (19)$$

(b_3 is the homogeneous part of the magnetic field and b_2 the heterogeneous part). Physically, this assumes that the magnetic energy dominates the kinetic energy. The magnetic field is strong and the field lines are weakly bended by the flow. Finally, the loss function is assumed to write

$$\tilde{\mathcal{L}} = \tilde{A}\tilde{T}. \quad (20)$$

Thus, at this stage no heating is included and only a phase of the evolution, during which the gas cools, is described. These limitations will be relaxed in the numerical simulations of Sect. 4. Under conditions (14)-(20) the idealized system corresponding to Eqs. (1-6) is shown to reduce to a single time dependent ordinary equation (Appendix A)

$$(\ddot{a} + b_3 b_2) a^\gamma = K_0 \exp(-\tilde{A}\tau) \quad (21)$$

with $K_0 = \ddot{a}(0) + b_3^0 b_2^0$, $a(0) = 1$, and

$$b_2(\tau) = \frac{b_2^0}{a} + b_1^0 a^0 \frac{\tau}{a}, \quad (22)$$

$$b_3(\tau) = \frac{b_3^0}{a} + \frac{(b_1^0)^2}{a} \int_0^\tau \int_0^{\tau'} b_2(\tau'') d\tau'' d\tau' + b_1^0 c^0 \frac{\tau}{a}. \quad (23)$$

The transverse velocity is equal to

$$\tilde{V}_y(\tau, x') = c(\tau) x' + d^0 \int F(x') dx'. \quad (24)$$

3.2. Physical interpretation

In the non-magnetized case, studied in paper I, Eq. (21) is

$$\ddot{a} a^\gamma = K_0 \exp(-\tilde{A}\tau). \quad (25)$$

It admits the following exact solution

$$a(t) = \exp\left(-\frac{\tilde{A}}{\gamma+1}\tau\right), \quad (26)$$

provided initially

$$\ddot{a}(0) = \left(\frac{\tilde{A}}{\gamma+1}\right)^2, \quad \dot{a}(0) = -\frac{\tilde{A}}{\gamma+1}. \quad (27)$$

Solution (26) has a clear physical meaning: the thermal energy is radiatively dissipated and $\rho = 1/a f(\tilde{x}/a)$ tends to a Dirac function (if $F(\infty) \neq \infty$).

Let us now consider the case of an initial density distribution weakly peaking at the origin (for instance a gaussian distribution). The case $\ddot{a}(0) < 0$ is unphysical because high densities correspond to low thermal pressures, which leads to an unphysical collapse. For similar reasons, we only consider initial conditions with, $K_0 = \ddot{a}(0) + b_3(0)b_2(0) > 0$ and

$b_3(0)b_2(0) < 0$, i.e. high densities (center) correspond to high thermal and magnetic pressure.

a) If the magnetic field is transverse ($b_1^0 = 0$) and the initial transverse velocity is equal to zero ($c^0 = 0, d^0 = 0$), then system of Eqs. (21-23) is as follows

$$b_2 = \frac{b_2^0}{a} \quad (28)$$

$$b_3 = \frac{b_3^0}{a} \quad (29)$$

$$\left(\ddot{a} + \frac{b_3^0 b_2^0}{a^2} \right) a^\gamma = K_0 \exp(-\tilde{A} \tau). \quad (30)$$

Hence, the magnetic field is proportional to the density and the ratio b_3/b_2 is constant. The condensation is prevented by the magnetic pressure through the term $b_3^0 b_2^0/a^2$ (in the following, we will simply refer to $b_3 b_2$ as the *magnetic pressure*). With $K_0 > 0$, we have

$$\ddot{a} + \frac{b_3^0 b_2^0}{a^2} > 0. \quad (31)$$

Thus, if $1/a$ increases strongly (condensation), so does \ddot{a} because $b_3^0 b_2^0 < 0$. Consequently, \dot{a} increases and tends to become positive, then $1/a$ tends to decrease (re-expansion).

b) If the magnetic field is oblique ($b_1^0 \neq 0$) and the initial transverse velocity is equal to zero ($c^0 = 0, d^0 = 0$)

$$b_2(\tau) = \frac{b_2^0}{a}, \quad (32)$$

$$b_3(\tau) = \frac{b_3^0}{a} + \frac{b_2^0 (b_1^0)^2}{a} \int_0^\tau \int_0^{\tau'} \frac{1}{a(\tau'')} d\tau'' d\tau', \quad (33)$$

$$\left(\ddot{a} + \frac{(b_2^0 b_1^0)^2}{a^2} \int_0^\tau \int_0^{\tau'} \frac{1}{a(\tau'')} d\tau'' d\tau' + \frac{b_3^0 b_2^0}{a^2} \right) a^\gamma = K_0 \exp(-\tilde{A} \tau). \quad (34)$$

The ratio b_3/b_2 is not constant anymore, and a new term appears in the l.h.s. of Eq. (34), which corresponds to a transverse velocity field generated by the magnetic tension. It contributes through the $\mathbf{B} \cdot \text{grad} \mathbf{V}$ term of Eq. (5) to the evolution of the transverse magnetic component. At $\tau = 0$, this term is equal to zero, then it grows and if $b_2 < 0$ and b_1^0 is large enough, b_3 decreases. If b_3 becomes comparable to b_2 the approximation stated in Eq. (19) is no longer valid.

c) When the transverse velocity is initially not zero (may be a consequence of the previous phase), the evolution may be more complex and will not be further considered here.

3.3. Numerical solution with a transverse and an oblique magnetic field

An analytical solution of Eq. (34) seems to be out of reach and numerical solution is now addressed. Let us consider the variable

$$\alpha = \int_0^\tau \int_0^{\tau'} \frac{1}{a} d\tau'' d\tau'. \quad (35)$$

Eq. (34) becomes

$$-\frac{d^4 \alpha}{dt^4} + \frac{2}{\tilde{\alpha}} \left(\frac{d^3 \alpha}{dt^3} \right)^2 + ((b_1^0 b_2^0)^2 \alpha + b_3^0 b_2^0) (\ddot{\alpha})^4 = K_0 (\ddot{\alpha})^{\gamma+2} \exp(-\tilde{A} \tau) \quad (36)$$

with

$$\alpha(0) = 0, \quad \dot{\alpha}(0) = 0, \quad \ddot{\alpha}(0) = \frac{1}{a(0)} = 1,$$

$$\frac{d^3 \alpha}{dt^3}(0) = -\frac{\dot{a}(0)}{a(0)^2}, \quad K_0 = \ddot{a}(0) + b_3^0 b_2^0.$$

We numerically solve this 4th order differential equation, using a 4th order Runge-Kutta method. For initial values close to the values given in Eq. (27), the non-magnetized case (described by Eq. 25) behaves very differently from the adiabatic one. Thus, we choose initial conditions near these two values ($\dot{a}(0) = -0.7$ and $\ddot{a}(0) = 9/16$ with $\tilde{A} = 2$). We explore two different magnetic cases: (1) case of a purely transverse magnetic field and (2) case of an oblique magnetic field. The results can be seen on Fig. 1. The adiabatic case ($\tilde{A} = 0$) and non adiabatic case ($\tilde{A} = 2$) without magnetic field are also shown for easier comparison.

While a strong condensation is observed in the absence of a magnetic field (paper I), the transverse field quickly stops the condensation. The case of the oblique field is subtly different, the contraction is effectively slowed down, but the magnetic pressure which initially increases, vanishes before the contraction stops (see Fig 2). Our weak heterogeneity approximation (Eq. 19) breaks down at this point and the solution cannot be further calculated. But the condensation is expected to proceed further, because the thermal energy has already been radiated away and the magnetic pressure is weak. Whether this *magnetic pressure leak* mechanism operates, depends on the initial magnitude of the longitudinal magnetic field, hence on the angle ω between the initial velocity and magnetic fields.

3.4. Magnetic pressure leak, efficiency as a function of the incidence angle

How does the magnetic pressure evolution depend on the magnetic intensity ($\sqrt{(b_1^0)^2 + (b_3^0)^2}$) and on the angle ω ? We investigate this issue in the oblique case just considered ($\dot{a}(0) = -0.7, \ddot{a}(0) = 9/16, \tilde{A} = 2$) by varying the initial values of b_1, b_2 and b_3 , in the weak heterogeneity case ($b_3^0/b_2^0 = -40$). In the purely transverse case, the ratio b_3/b_2 stays constant, while $|b_2 b_3|$ steadily increases during the compression, preventing compression far beyond the pressure equilibrium point. On the opposite, we saw (Fig. 2) that the *magnetic pressure* $|b_2 b_3|$ rapidly decreases before the compression stops in the oblique case considered. Using this sudden decrease as condensation criterion we can draw the condensation threshold line, in the (B, ω) plane (Fig. 3) for the selected initial conditions. This qualitative criterion constitutes a first approach towards an understanding of the condensation conditions. Calculations have

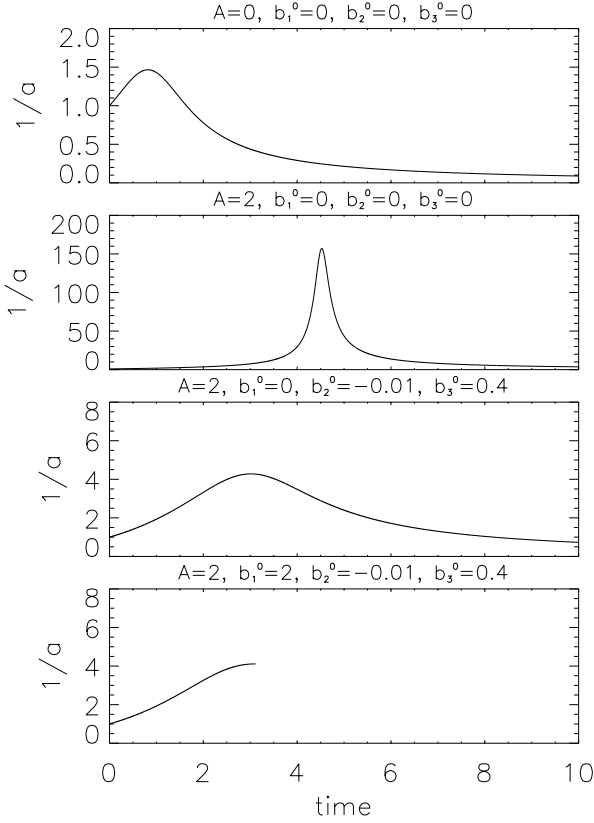


Fig. 1. Numerical resolution of Eq. (34) in four different cases. The normalised density at origin $1/a$, is plotted as a function of τ , the a dimensional time. The two upper panels display the non-magnetised solutions of paper I, the adiabatic and cooling cases respectively. The thermal approximation breaks down for large densities. The two lower panels display solutions with a magnetic field. Third panel: the transverse magnetic field prevents the condensation. Fourth panel: a longitudinal field has been added. Unfortunately, the approximation stated in Eq. (19) is no longer valid after $\tau \simeq 3$ and the computation cannot be continued. The essential difference between the third and fourth panel nevertheless appears clearly in Fig. 2.

not been carried on for $\sqrt{(b_1^0)^2 + (b_3^0)^2} < 2$, as in these cases the approximation of a weakly heterogeneous field is not appropriate. This situation will be covered in the simulation presented in the next section.

In the conditions explored, the maximum angle ω_{\max} increases with the magnetic field intensity.

We conclude that:

- i) In a one dimensional condensation process with an initial transverse velocity field equal to zero, the magnetic pressure starts to increase and can possibly decrease before re-expansion if the initial flow angle with respect to the magnetic field, ω , is small enough (see Fig. 2).
- ii) In this case, the higher the magnetic intensity is and the smaller the angle ω , the faster the decrease of the magnetic pressure will be.
- iii) Whatever the intensity of the magnetic field, the condensation process is still possible if the angle ω is below a maximum value: ω_{\max} . For weak magnetic fields, the magnetic

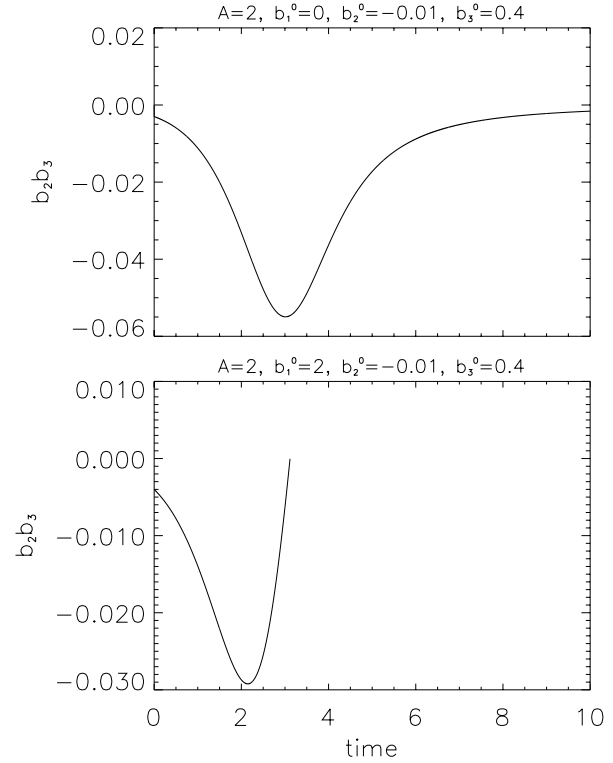


Fig. 2. Evolution of the magnetic pressure : b_2b_3 in the two magnetized cases of Fig. 1 ($b_1^0 = 0$ and $b_1^0 = 2$). In the first case, the magnetic pressure is proportional to $1/a^2$ (ρ^2). In the second case, the behaviour is more complex. $|b_2b_3|$ starts to increase but then decreases whereas density still increases (see Fig. 1). Before it becomes equal to zero, the approximation stated in Eq. (19) breaks down.

pressure has small effect on the dynamics and the condensation process can occur even for large values of ω . For large magnetic fields, ω_{\max} increases with $|\mathbf{B}|$ (see Fig. 3).

4. Numerical simulations

4.1. The simulation

The formalism and the results presented in the previous section allow us to qualitatively understand the behaviour and the effects of the magnetic field in a converging and very compressible flow. Except for the solutions of Appendix B, they are only valid for loss functions proportional to temperature ($\mathcal{L} \propto T$) and this is an important restriction. In particular, these functions present no thermal bistability. In order to avoid this restriction and to understand more quantitatively the thermal condensation in a bistable flow like the ISM, we now present a numerical simulation of the system of Eq. (1-6). As in paper I, the cooling function is a fit (Liou 1991) of the function calculated by Dalgarno & McCray (1972) and is equal to:

$$\Lambda(T) = 8.31 \cdot 10^{-39} \text{J m}^3 \text{s}^{-1} \exp(-480 \text{K}/T) + 2.73 \cdot 10^{-35} \text{J m}^3 \text{s}^{-1} \exp(-(\log(T/80.2 \text{K}) - 7.6)^2) \quad (37)$$

The heating rate per atom is taken as a constant equal to $2 \cdot 10^{-32} \text{W}$ ($2 \cdot 10^{-25} \text{erg s}^{-1}$), and the ionization fraction is equal

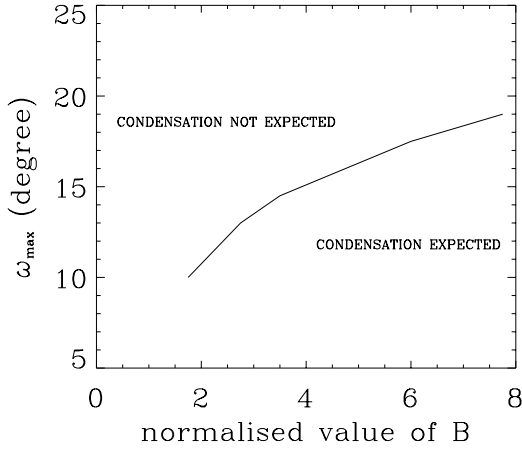


Fig. 3. Dependence of ω_{\max} with the initial magnetic intensity ($\sqrt{(b_1^0)^2 + (b_3^0)^2}$) (first approach). The points below this curve are expected to lead to a condensation because the magnetic pressure is weak, whereas the points above will not give such condensations because the gas re-expands before the magnetic pressure decreases sufficiently. For small values of the magnetic field our criterion is invalid, the magnetic pressure is low and the condensation is possible independently of ω .

to 10^{-3} . The resulting loss function is bistable and comparable to more recent calculations (Wolfire et al. 1995).

The main difficulty of the present problem is due to the presence of several very different time and space scales. The smallest space scale in the simulation is the Field length in the CNM (10^{-3} pc), and the largest is the scale of the initial flow. This difficulty is overcome by the use of an adaptive spatial grid with adaptive time steps. A description of the code can be found in paper I. The condition for adapting the resolution is that the spatial gradients of density and temperature must be smaller than 1%. Tests of the robustness of the results with respect to this criterion have been made for a simulation (not very close to the condensation threshold) with a tolerance of respectively 0.5% and 2%. The differences between these and the original results never exceed 1 and 2% respectively for any of the ρ , T , P , \mathbf{V} and \mathbf{B} fields. The total energy (thermal, kinetic and magnetic), the mass and the transverse magnetic flux (which is conserved in slab geometry) are conserved with an accuracy better than 10^{-4} . The comparison between numerical and approximate theoretical values of the fronts velocity gives agreement of 3%.

As in paper I, the simulations start from WNM with initially uniform density and temperature. The converging velocity field has no initial transverse component (see Fig. 4). The gas is initially linearly thermally stable. The initial magnetic field is also uniform and is defined by its intensity and the angle ω .

4.2. Cloud formation with magnetic field

We present two simulations that differ only in the initial values of ω and choose initial conditions (amplitude and typical spatial scale of the velocity field, thermal pressure) that would lead to thermal condensation in the absence of a magnetic field. The initial value of $|\mathbf{B}|$ is equal to $5 \cdot 10^{-10} T$ ($5 \mu\text{G}$), which is

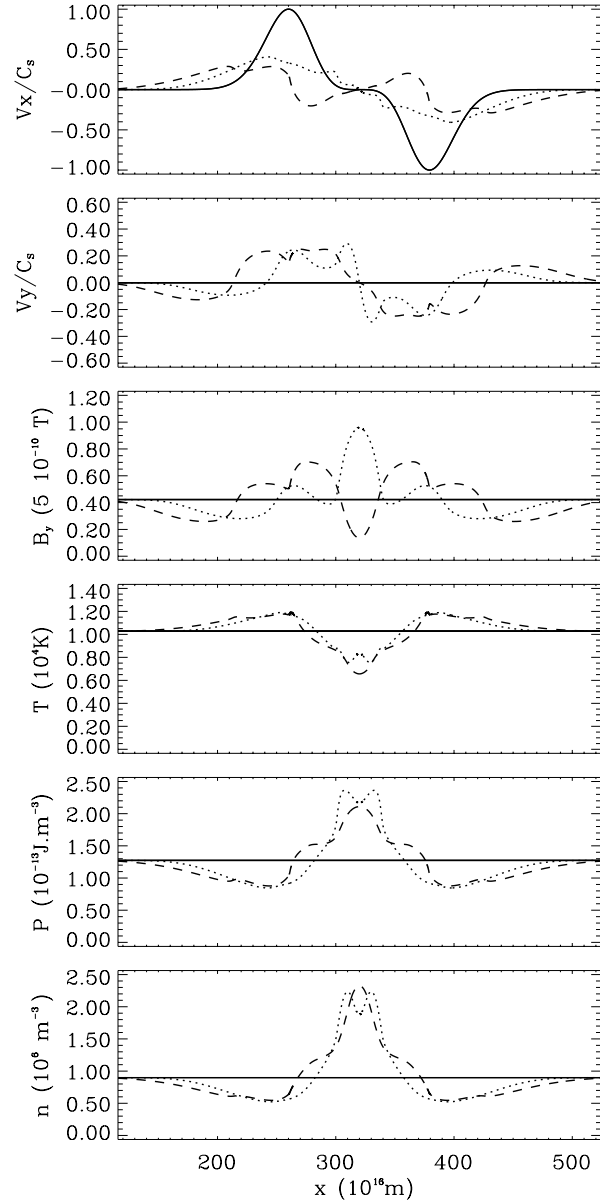


Fig. 4. The six fields considered for $\omega = 25^\circ$ and initial magnetic intensity equal to $5 \cdot 10^{-10} T$ ($5 \mu\text{G}$). Time 0 (full line), 42.40 (dotted line) and $72.43 \cdot 10^{12} \text{ s}$ (dashed line). After a short contraction, the gas re-expands and no thermal condensation occurs. However, at time 42.40 and at the center point, B_y/B_{y0} and ρ/ρ_0 are comparable, whereas at time 72.43 , B_y/B_{y0} is less than 1 and ρ/ρ_0 is greater than 2. Magnetic field and density decorrelate rapidly.

comparable to the measurements of Troland & Heiles (1986) and Myers et al. (1995). The results can be seen in Fig. 4 and Fig. 5.

For $\omega = 25^\circ$, the thermal condensation is not obtained, magnetic pressure prevents it. At time $t = 42.40 \cdot 10^{12} \text{ s}$ B_y and ρ are correlated, whereas at time $72.43 \cdot 10^{12} \text{ s}$ the central density peak corresponds to a minimum of B_y .

For $\omega = 15^\circ$ part of the gas, initially WNM, condenses into CNM, forming a cloud. As in the lower panel of Fig. 2, the magnetic tension is strong enough to force the magnetic pressure to

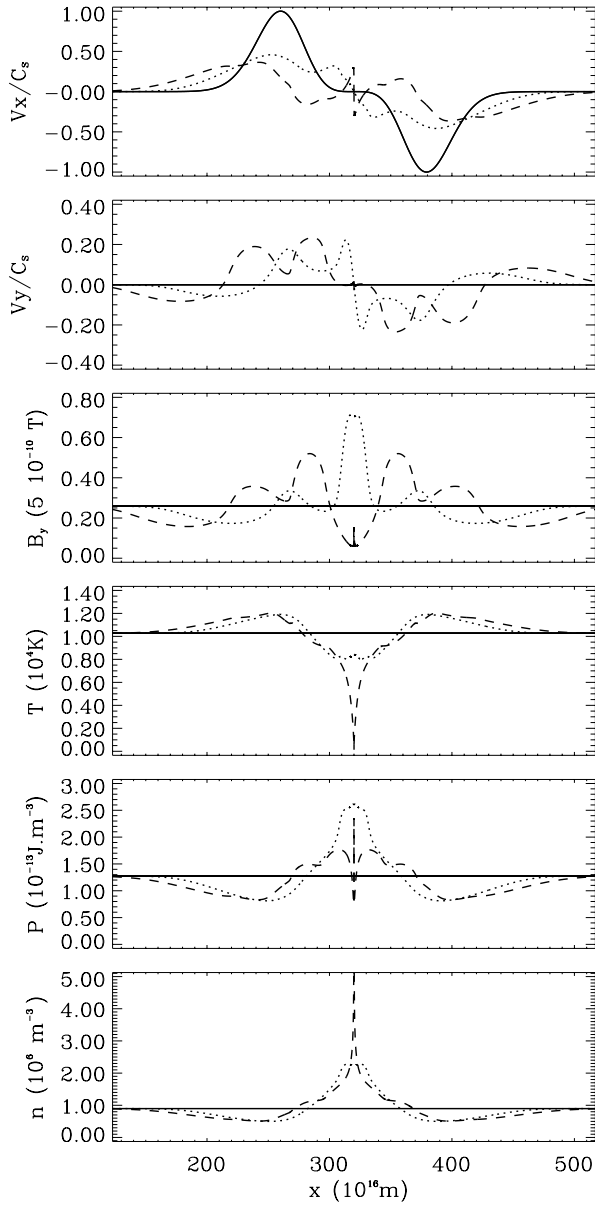


Fig. 5. The six fields considered for $\omega = 15^\circ$ and $|\mathbf{B}| = 5 \cdot 10^{-10} \text{ T}$ ($5 \mu\text{G}$). Time 0 (full line), 39.62 (dotted line) and $73.83 \cdot 10^{12} \text{ s}$ (dashed line). At time 73.83, very stiff gradients appear, due to the condensation of WNM into CNM. At time 39.62, the value of B_y at the center is about 3 times the initial value, which is also the ratio between density at origin and initial density. At time 73.83, B_y is about 3 times less than the initial value whereas the ratio between density at the center and initial density is greater than 150 (see Fig. 7).

decrease after an increase phase before the flow stops. Hence, the thermal condensation is possible. This highly compressible MHD process is more clearly illustrated in Fig. 6. The magnetic field lines and the velocity field of Fig. 5 are displayed in the x - y plane for three different times. The magnetic field lines are first bended forward by the longitudinal flow and the gas is put in forward motion ahead of the compression, first towards positive y , then towards negative y , when the field tension reverses the flow (upper panel). This side flow advects the field lines and inverts

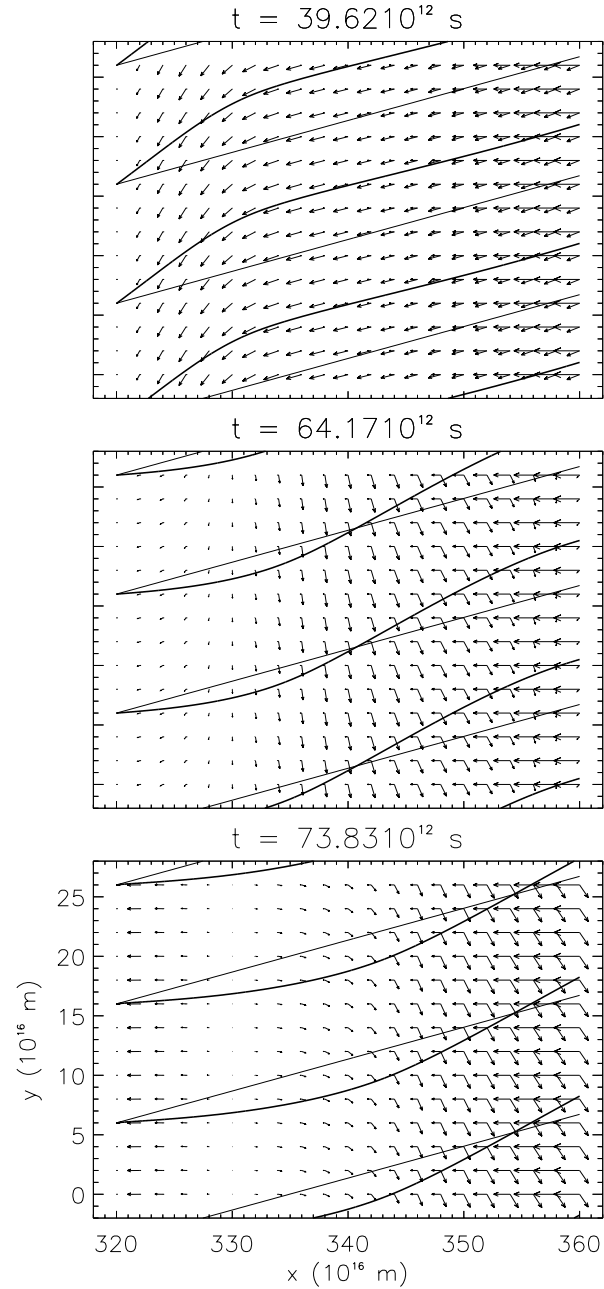


Fig. 6. Two dimensional display of Fig. 5 (half part only). Magnetic field lines and velocity field are presented for three different times. The initial conditions are superimposed for easier reference (thin lines).

their curvature in the neighbourhood of the convergence focus (middle panel), where the flow nearly stops. But the density in the center has been sufficiently increased in the meanwhile, for the thermal pressure drop to start pumping the neighbouring gas towards the center along the field lines, as clearly appears in the lower panel. The lines slowly unbend at subsequent times.

Simulations with a twice stronger field show a similar initial field bending, but the field relaxes much faster to its original direction, aligning the whole flow parallel to itself.

Fig. 7 is a spatio-temporal zoom of Fig. 5. The density reached in the center is more than a hundred times the den-

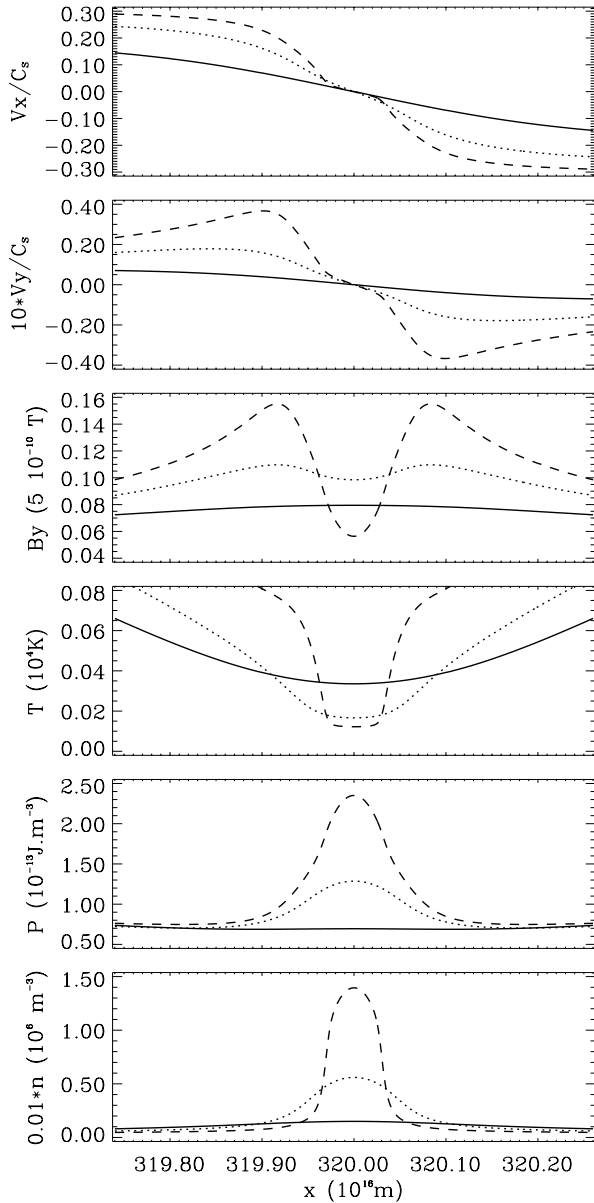


Fig. 7. Spatio-temporal zoom around the center of the simulation of Fig. 5 at time 72.15 (full line), 73.21 (dotted line) and 73.83 10^{12} s (dashed line), the spatial scale considered is a thousand times smaller than the scale of Fig. 5. The density increases up to $150 \cdot 10^6 \text{ m}^{-3}$ (150 cm^{-3})

sity of the WNM, whereas the value of the transverse magnetic field is comparable to the initial value. For this last example, we can conclude that the presence of a magnetic field does not prevent strong condensations.

The self-similar behaviour of the fields is apparent at times 72.15 and 73.21 10^{12} s (Fig. 7). The time evolution can be approximatively described by a spatial dilatation and renormalization of the different fields. It progressively disappears when part of the gas reaches thermal equilibrium because at this point the thermal loss function much deviates strongly from $\mathcal{L} \propto T$.

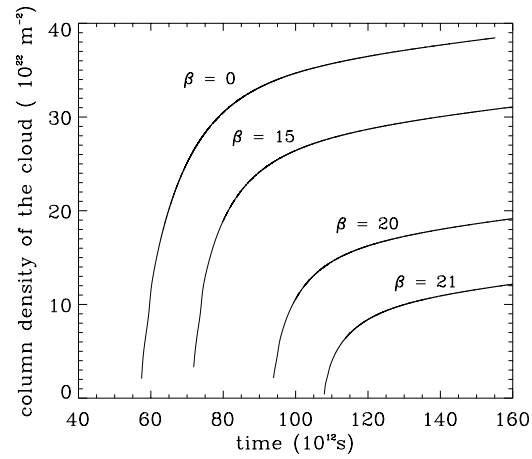


Fig. 8. Evolution of the column density of the cloud. All corresponding initial parameters are defined as in Fig. 4 except ω . Top curve is $\omega = 0^\circ$, second one $\omega = 15^\circ$, third and fourth one, 20° and 21° respectively. For $\omega = 22^\circ$ no thermal condensation occurs. As expected, the condensation starts later and is less efficient when ω increases.

4.3. Cloud evolution with magnetic field

Let us further investigate the consequences of the magnetic field during the condensation process. Fig. 8 shows the evolution of the cloud column density (only pixels with density 10 times higher than the initial density are taken into account) for four values of ω . The condensation occurs later when ω increases, and is less efficient. However, the growth curves are similar for all angles, starting with a fast dynamical growth followed by a slow conductive growth (not well described because in our simulation κ does not depend on \mathbf{B}). To allow for the first parcel of gas (WNM) to reach the second branch of equilibrium (CNM), the magnetic pressure has to be small. According to the mechanism described in Sect. 2 and 3 it is more difficult and slower to decrease the magnetic pressure when the value of ω increases. But, once the condensation process starts, the effect of the magnetic field on the growth of the cloud becomes weak.

The evolution of the cloud formed in Fig. 7, is shown in Fig. 9 at subsequent times. Most of the gas in the cloud reaches thermal equilibrium, two fronts separate the two phases. Pressure and density decrease slowly and the cloud relaxes until it reaches pressure equilibrium with the surrounding medium. The fronts propagate slowly in a quasi-isobaric regime (see Ferrara & Shchekinov 1993 and paper I for a quantitative comparison in the non-magnetized case). Due to a small transverse velocity gradient (induced by the magnetic tension), the transverse magnetic field, that decreased during the condensation process, rises back to the mean large scale value. The field lines slowly unbend until they become straight. At the end of the process, thermal and magnetic pressure are uniform.

4.4. Threshold dependence on magnetic and velocity fields

We now investigate the condensation dependence on magnetic intensity and velocity amplitude. In paper I, we already studied how the nucleation threshold varies with the initial pres-

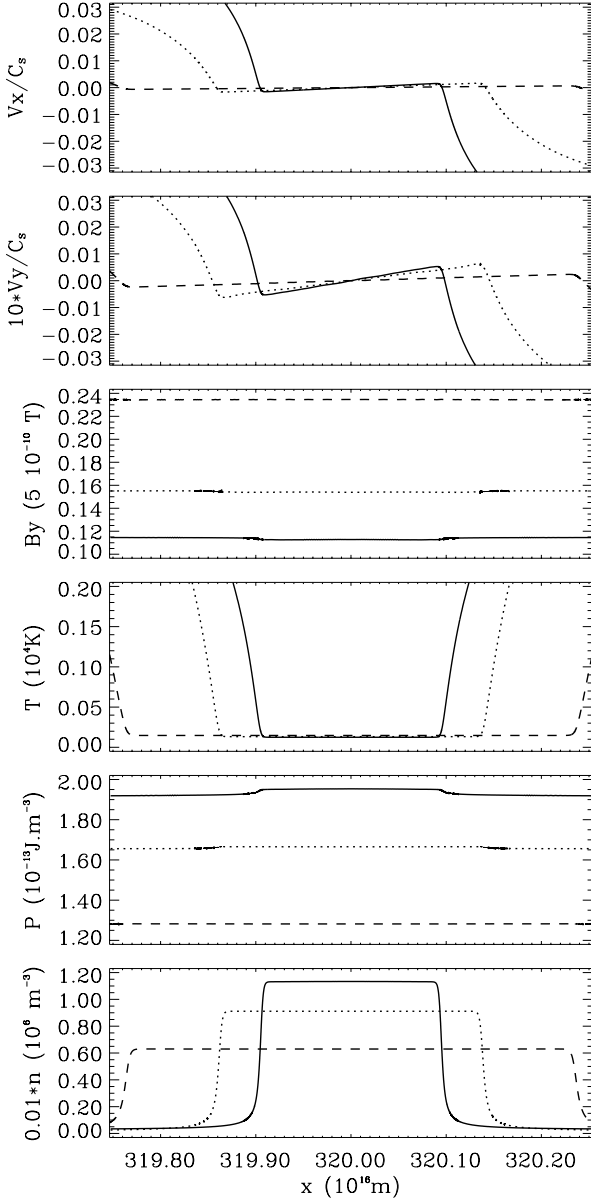


Fig. 9. Long time evolution of the cloud formed in Fig. 5 for time 84.9 (full line), 96.2 (dotted line) and $142.3 \cdot 10^{12}$ s (dashed line). The density decreases and the temperature is constant so that thermal pressure decreases until the gas reaches pressure equilibrium with the surrounding medium. The transverse magnetic field re-increases until it reaches the average large scale value.

sure, amplitude and size of the convergent flow. We shall not consider it further in this paper, although an extended study including these parameters and the magnetic field has to be done at some stage. The initial pressure $P_0 = 1.27 \cdot 10^{-13} \text{ J m}^{-3}$ ($1.27 \cdot 10^{-12} \text{ erg cm}^{-3}$) and the initial size of the convergent flow is $16 \cdot 10^{17} \text{ m}$ ($\simeq 40 \text{ pc}$) (twice the distance between the center and the peaks of the initial velocity field). These two values are typical of the WNM. For several values of $|\mathbf{B}|$ and for the two values $V_{x,\text{max}}/C_s = 1$ and $V_{x,\text{max}}/C_s = 1.2$, we look for the largest value of ω , ω_{max} at which thermal condensation occurs. The method used is dichotomy and the accuracy is one

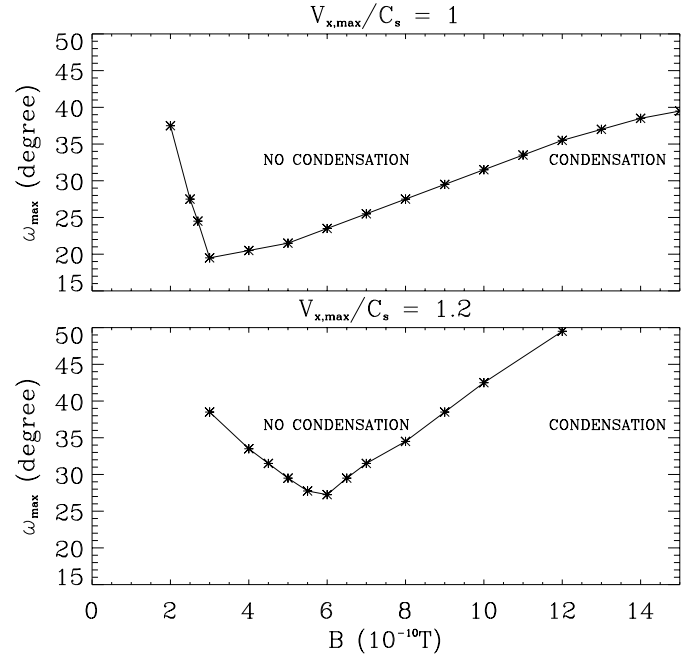


Fig. 10. Dependence of ω_{max} on initial magnetic intensity $|\mathbf{B}|$ for two initial values of $V_{x,\text{max}}/C_s$. In both cases two branches can be seen: the condensation does not occur at intermediate values of B . When the initial velocity increases, the minimum value of ω_{max} increases also, the condensation is easier.

degree. The results are presented on Fig. 10. In both cases two branches are found, between which no condensation occurs.

Before making further comments on Fig. 10, we use Eq. (13) to derive a rough expression of the magnetic field that allows us to understand qualitatively some features of Fig. 10 and summarizes the conclusions *i*), *ii*) and *iii*) of Sect. 3. The l.h.s. of Eq. (13) is comparable to $B_y(0)l(0)$ and the first term of the r.h.s. to $B_y(t)l(t)$. The order of magnitude of the second term of l.h.s. is given by $(B_x^2/\mu_0) B_y(t) \tau^2/(\rho(t)l(t))$ where $\tau \simeq l_0/v$ is the dynamical time. The matter conservation leads to $l(0)\rho(0) = l(t)\rho(t)$. With these relations, we find

$$B_y \simeq B_y(0) / \left(\frac{\rho_0}{\rho} + \frac{B_x^2/\mu_0}{\rho_0 v^2} \right). \quad (38)$$

If $B_x^2/\mu_0 \rho_0 v^2 \rightarrow \infty$, clearly Eq. (38) is not valid anymore.

With Eq. (38) three regimes are expected:

- weak magnetic fields, $B_x^2/\mu_0 < \rho_0 v^2$: B_y is independent of B_x and almost proportional to density; ω_{max} rapidly decreases with $|\mathbf{B}|$ because of the magnetic pressure.
- strong magnetic fields, $B_x^2/\mu_0 > \rho_0 v^2$: B_y is no longer proportional to ρ , its evolution depends on B_x , and ω_{max} increases with $|\mathbf{B}|$. This result is in good qualitative agreement with the analytical result (Fig. 3). The poor quantitative agreement is due to the significant differences between the thermal processes considered in the two approaches.
- The minimum ω_{max} is found for an intermediate value of the magnetic field: $B_x^2/\mu_0 \simeq \rho_0 v^2$. There is a rough equipartition between magnetic and other energies (thermal and ki-

netic). When the kinetic energy increases, so does the value of $|\mathbf{B}|$ corresponding to the minimum ω_{\max} .

The typical values of ω_{\max} range from 20 to 40°.

The distribution of ω results from the development of the MHD turbulence and is not straightforwardly quantified. The assumption of a random distribution likely yields an upper limit on the efficiency loss (r_{mag}) with respect to the unmagnetized cases. We have:

$$r_{\text{mag}} = \int_0^{\omega_{\max}} \sin \omega \, d\omega = 1 - \cos \omega_{\max} \quad (39)$$

$\omega_{\max} = 20$ gives $r_{\text{mag}} = 6\%$ and $\omega_{\max} = 40$, $r_{\text{mag}} = 23\%$. As expected the magnetic field stabilizes partially the flow against thermal condensation, reducing the number of condensations that would occur in a non-magnetized gas by a factor 5 to 20. However, the condensations are still possible, the rate of cloud formation is reduced but is not equal to zero.

For larger velocities, several structures appear and the problem becomes more complex because these structures collide. Such cloud collisions, well described in the literature (Mac Low et al. 1994, Ricotti et al. 1997, Miniati et al. 1999), lead to strong density contrasts in the CNM and strong enhancement of the local magnetic field.

5. Discussion

Self-similar solutions have been derived in Sect. 3 for a converging and cooling MHD flow. A magnetic transverse component, as expected, reduces and possibly stops the condensation, but a sufficient longitudinal component is able to force the alignment of the velocity and magnetic fields, hence reducing the magnetic pressure without stopping the condensation process. The numerical results of Sect. 4, obtained for interstellar thermally bistable gas, confirm this behaviour. The dynamically induced thermal condensation, described in paper I, is possible when the angle between the initial magnetic and velocity fields ω is smaller than a maximum value, ω_{\max} , which depends on the magnetic field intensity and flow parameters. This maximum angle lies in the range 20 to 40° for ISM conditions. Except for this important restriction, the mechanism presented in paper I remains almost unchanged. If the initial value of the maximum velocity reaches a critical value, thermal condensation occurs, with a fast dynamical growth phase and a slow conductive phase. If the mean thermal pressure is above the equilibrium pressure (value of the pressure at which the fronts do not propagate), the cloud further grows during the conductive phase, while it evaporates in the opposite case.

During the fast dynamical phase, the value of the transverse magnetic field starts to increase, then decreases possibly below the mean large scale value and finally slowly reincreases during the subsequent slow evolution until it reaches the mean large scale value. As a consequence in a non-gravitational thermally bistable flow, there is no correlation between the density of the gas and the magnetic field. The magnetic intensity is moderately affected by the evolution of the density, as long as violent

compressions are considered (shocks, cloud collisions), and relaxes to the original value in both phases. Indeed, in a medium with an approximate equipartition between thermal and magnetic pressure, like the neutral ISM, a correlation between field intensity and density would prevent the cloud formation. This result agrees with the observational conclusions of Troland & Heiles (1986), who find no increase of magnetic field for densities between 10^5 and 10^8 m^{-3} (0.1 to 10^2 cm^{-3}).

The typical column density of the clouds created by dynamically induced thermal condensation is in the range 10^{23} - 10^{24} m^{-2} (10^{19} - 10^{20} cm^{-2}), which are typical column densities for observed HI clouds (Kulkarni & Heiles 1987, Dickey & Lockman 1990) or filaments of interstellar cirrus (Joncas et al. 1992). This double agreement with observational data favours the proposed mechanism as actively participating to the formation of interstellar cirrus.

Passot et al. (1995) find that the magnetic field is more intense on average (small values are found also) and more turbulent in the dense regions than in the diffuse ones (see also Ballesteros et al. 1999). But we believe that the physical situations they consider are not directly comparable to ours. Their flows are continuously thermally stable between 10^2 and 10^4 K and consequently the denser parts (the clouds) have necessarily a higher thermal pressure at thermal equilibrium than the gas of low density (the intercloud medium). The structures are transient and the distinction between the diffuse phase and the dense phase is not clear-cut. The structures are dynamically formed and dynamically maintained and cannot relax into a stationary regime. On the contrary, as we showed in the previous section, the bistable behavior allows the formation of long lived structures and has deep consequences on the evolution of the velocity and magnetic fields. However we did not consider here a problem as general as the situation described by Passot et al. Our simulation is one dimensional only and we focused on the formation of one single cloud. In a more general higher dimensional situation with a MHD turbulent flow and with several clouds formed in the gas, it could be possible that the clouds never reach mechanical equilibrium and that highly dynamical effects like cloud collisions often occur and dominate the dynamics.

In their simulation, Passot et al. note that the stellar formation rate (which follows the rate of condensation) starts to decrease when the value of the magnetic field increases, then increases and finally decreases again. We believe, that the first decrease and subsequent enhancement of stellar formation with the magnetic field are likely, at least in part to be, due to the mechanism pointed out here. Condensations are easier when $|\mathbf{B}|$ is greater than the equipartition value. We did not find the saturation that they have identified at large intensities. A reason of this may be the absence of gravity in our simulation. Gravity can produce contraction of the gas even perpendicularly to the field lines. But, if the magnetic field is strong these contractions are not possible, and the rate of strong condensation is reduced.

Apart from the magnetic field, all the limitations listed in the discussion of paper I still apply. Not least, in the case of the neutral interstellar medium, the chemistry of H_2 will play a

significant role and should be included. In spite of these limitations, we believe that the dynamically induced thermal condensation is a key in the description of thermally bistable flows like the neutral ISM. The magnetic field introduces, as expected, a strong anisotropy in the medium, but it does not prevent thermal condensation. In a trans-sonic flow, stable clouds with the same mean magnetic field as the intercloud medium can be easily formed.

Acknowledgements. We thank Christophe Dupraz for a critical reading of the manuscript, Thierry Passot and Enrique Vázquez-Semadeni for stimulating discussions and Mordecai-Mark Mac Low, the referee, for his help in improving the original manuscript.

Appendix A: solution of a magneto-thermal condensation for weakly heterogeneous magnetic fields

In this Appendix, assuming that the magnetic field is weakly heterogeneous and neglecting viscosity and conduction, we show that the idealized system corresponding to Eqs. (1-6) admits self-similar solutions. These solutions derive from the resolution of one single time ordinary differential equation. We use the adimensional variables defined in Sect. 3.1 and look for self-similar solutions as defined in Eqs. (14-15). Partial derivatives are simply related, for any function G of the reduced spatial coordinate \tilde{x}/a

$$\partial_\tau G(\tilde{x}/a) + \frac{\dot{a}}{a} \tilde{x} \partial_{\tilde{x}} G(\tilde{x}/a) = 0. \quad (\text{A.1})$$

The integration of the x-momentum equation gives the total pressure \tilde{P}_T

$$\tilde{P}_T = \tilde{P} + \frac{\tilde{B}_y^2}{2} = -\ddot{a} \int_0^{x'} f(u) u du + \tilde{P}_c(\tau), \quad (\text{A.2})$$

where $\tilde{P}_c(\tau)$ is the pressure at origin. We define

$$F(x') = \int_0^{x'} f(u) u du. \quad (\text{A.3})$$

Consequently, the temperature is given by

$$\tilde{T} = a \left(-\ddot{a} \frac{F(x')}{f(x')} + \frac{\tilde{P}_c}{f(x')} - \frac{\tilde{B}_y(x', \tau)^2}{2f(x')} \right). \quad (\text{A.4})$$

Although exact solutions exist with a magnetic field equal to (see Appendix C).

$$\tilde{B}_y(x', \tau) = B_2(\tau) \sqrt{F(x')}, \quad (\text{A.5})$$

the magnetic field vanishes at the center and contributes to the compression of the gas instead of opposing to the condensation, as would be expected. We then rather search for magnetic fields equal to

$$\tilde{B}_y(x', \tau) = b_3 + b_2 F(x'); \quad (\text{A.6})$$

b_3 is the homogeneous part of the magnetic field and b_2 is the heterogeneous one. Eq. (4), in its one dimensional form, is as follows

$$\partial_\tau \tilde{T} + \frac{\dot{a}}{a} \tilde{x} \partial_{\tilde{x}} \tilde{T} + \frac{\dot{a}}{a} (\gamma - 1) \tilde{T} = -\tilde{\mathcal{L}}. \quad (\text{A.7})$$

Considering the expression of the temperature (A.4), of the magnetic field (A.6) and the property (A.1), we obtain

$$\begin{aligned} & \left(\frac{d}{d\tau} (a\tilde{P}_c - \frac{1}{2}ab_3^2) + (\gamma - 1) \frac{\dot{a}}{a} (a\tilde{P}_c - \frac{1}{2}ab_3^2) \right) \frac{1}{f(x')} - \\ & \left(\frac{d}{d\tau} (\ddot{a}a + b_3b_2a) + (\gamma - 1) \frac{\dot{a}}{a} (\ddot{a}a + b_3b_2a) \right) \frac{F(x')}{f(x')} - \\ & \left(\frac{d}{d\tau} (\frac{1}{2}ab_2^2) + (\gamma - 1) \frac{\dot{a}}{a} (\frac{1}{2}ab_2^2) \right) \frac{F(x')^2}{f(x')} = -\tilde{\mathcal{L}}. \quad (\text{A.8}) \end{aligned}$$

In the general case, the three terms of the l.h.s., which have functionally independent spatial variations, lead to three time differential equations. As we will see later two additional constraints can be set on b_2 and b_3 . Thus, with five constraints and four variables there is no solution in the general case. In Appendix B, we find exact solutions in the case $\gamma = 2$ and for a special choice of the loss function. Here, to overcome this difficulty, we assume that:

$$b_3 \gg b_2 F(x'). \quad (\text{A.9})$$

This means that the magnetic field is weakly heterogeneous. We then can neglect the third term of the l.h.s. in Eq. (A.8). Even with this assumption, Eq. (A.8) admits solutions only for special loss functions. As in paper I, we consider the loss function: $\tilde{\mathcal{L}} = \tilde{A} \tilde{T}$, which has been shown to be in reasonable agreement with a more realistic simulation during the strong condensation phase. It is also possible to add a term proportional to a powerlaw of density to this loss function, but special density distributions f are then required (see Appendix B). With this restriction Eq. (A.8) implies

$$\begin{aligned} \frac{d}{d\tau} (a\tilde{P}_c - \frac{1}{2}ab_3^2) + (\gamma - 1) \frac{\dot{a}}{a} (a\tilde{P}_c - \frac{1}{2}ab_3^2) = & \quad (\text{A.10}) \\ -\tilde{A} (a\tilde{P}_c - \frac{1}{2}ab_3^2), \end{aligned}$$

$$\begin{aligned} \frac{d}{d\tau} (\ddot{a}a + b_3b_2a) + (\gamma - 1) \frac{\dot{a}}{a} (\ddot{a}a + b_3b_2a) = & \quad (\text{A.11}) \\ -\tilde{A} (\ddot{a}a + b_3b_2a). \end{aligned}$$

Integrating once, we obtain

$$(\tilde{P}_c - \frac{1}{2}b_3^2) a^\gamma = Q_0 \exp(-\tilde{A} \tau), \quad (\text{A.12})$$

$$(\ddot{a} + b_3b_2) a^\gamma = K_0 \exp(-\tilde{A} \tau), \quad (\text{A.13})$$

with $Q_0 = P_c(0) - \frac{1}{2}b_3(0)^2$, $K_0 = \ddot{a}(0) + b_3(0)b_2(0)$ and $a(0) = 1$. One has to keep in mind that these equations assume that the magnetic field is weakly heterogeneous (Eq. A.9). We will not consider further Eq. (A.12) because it describes only a uniform component that has no effect on the dynamics.

The evolution of the magnetic field is given by Eq. (5) and Eq. (6). For the x-component, they lead to

$$\partial_\tau \tilde{B}_x + \frac{\dot{a}}{a} \tilde{x} \partial_{\tilde{x}} \tilde{B}_x = 0, \quad \partial_{\tilde{x}} \tilde{B}_x = 0, \quad (\text{A.14})$$

and $\tilde{B}_x = b_1^0$ is constant. For the y-component, we have

$$\dot{b}_3 + \dot{b}_2 F(x') - b_1^0 \partial_x \tilde{V}_y + \frac{\dot{a}}{a} (b_3 + b_2 F(x')) = 0, \quad (\text{A.15})$$

Let us consider the y-component of Eq. (2)

$$\partial_\tau \tilde{V}_y + \frac{\dot{a}}{a} \tilde{x} \partial_x \tilde{V}_y = b_1^0 b_2 \frac{F'(x')}{f(x')}. \quad (\text{A.16})$$

This equation integrates to

$$\tilde{V}_y(\tau, x') = c(\tau)x' + M(x'), \quad (\text{A.17})$$

$$\dot{c} = b_1^0 b_2. \quad (\text{A.18})$$

and any function M is allowed. From Eqs. (A.15, A.17, A.18) one derives

$$\dot{b}_2 + \frac{\dot{a}}{a} b_2 - d^0 b_1^0 \frac{1}{a} = 0, \quad (\text{A.19})$$

$$\dot{b}_3 + \frac{\dot{a}}{a} b_3 - b_1^0 \frac{c}{a} = 0, \quad (\text{A.20})$$

where d^0 is a constant and $M'(x') = d^0 F(x')$. These two equations can be integrated and lead to

$$b_2(\tau) = \frac{b_2^0}{a} + b_1^0 d^0 \frac{\tau}{a}, \quad (\text{A.21})$$

$$b_3(\tau) = \frac{b_3^0}{a} + \frac{(b_1^0)^2}{a} \int_0^\tau \int_0^{\tau'} b_2(\tau'') d\tau'' d\tau' + b_1^0 c^0 \frac{\tau}{a}.$$

Finally, with Eq. (A.13)

$$(\ddot{a} + b_3 b_2) a^\gamma = K_0 \exp(-\tilde{A} \tau).$$

The system of Eq. (1-6) in its ideal version with cooling only is reduced to a single time dependent equation.

Appendix B: exact solution of a magneto-thermal condensation

In this appendix, we find an exact solution in the idealised limit of Eq. (1-6) in the case where the adiabatic index γ is equal to 2. We start as in Appendix A and consider Eq. (A.8). In the case $d^0 = 0$, Eq. (A.21) leads to

$$b_2 = \frac{b_2^0}{a}. \quad (\text{B.1})$$

If $\gamma = 2$, the third term of l.h.s. of Eq. (A.8) is equal to zero. We consider a loss function equal to

$$\tilde{\mathcal{L}} = -\tilde{\Gamma} + \tilde{A} \tilde{T} + \tilde{C} \tilde{\rho}. \quad (\text{B.2})$$

The thermal equilibrium condition leads to the relation

$$\tilde{P} = \frac{\tilde{\Gamma}}{\tilde{A}} \tilde{\rho} - \frac{\tilde{C}}{\tilde{A}} \tilde{\rho}^2. \quad (\text{B.3})$$

Thus, for $\tilde{\rho} = \tilde{\rho}_{\text{crit}} = \tilde{\Gamma}/2\tilde{C}$, we have

$$\left(\frac{\partial \tilde{P}}{\partial \tilde{\rho}} \right)_{\tilde{z}=0} = 0. \quad (\text{B.4})$$

If $\rho < \rho_{\text{crit}}$ the gas is linearly thermally stable and unstable in the opposite case. Eq. (A.8) becomes

$$\begin{aligned} & \left(\frac{d}{d\tau} (a\tilde{P}_c - \frac{1}{2}ab_3^2) + (\gamma - 1) \frac{\dot{a}}{a} (a\tilde{P}_c - \frac{1}{2}ab_3^2) \right) \frac{1}{f(x')} - \\ & \left(\frac{d}{d\tau} (\ddot{a}a + b_3 b_2 a) + (\gamma - 1) \frac{\dot{a}}{a} (\ddot{a}a + b_3 b_2 a) \right) \frac{F(x')}{f(x')} = \\ & \tilde{\Gamma} - \tilde{A} \left((a\tilde{P}_c - \frac{1}{2}ab_3^2) \frac{1}{f(x')} - (\ddot{a}a + b_3 b_2 a) \frac{F(x')}{f(x')} \right. \\ & \quad \left. - \frac{1}{2} \frac{(b_2^0)^2}{a} \frac{F(x')^2}{f(x')} \right) - \frac{\tilde{C}}{a} f(x'). \end{aligned} \quad (\text{B.5})$$

Let us consider a gaussian distribution of density: $f(x') = \tilde{\rho}_0 \exp(-(x'/\tilde{x}_0)^2)$. One has

$$F(x') = \int_0^{x'} z f(z) dz = \frac{\tilde{x}_0^2}{2} (\tilde{\rho}_0 - f(x')). \quad (\text{B.6})$$

We have the identities

$$\begin{aligned} \frac{F(x')^2}{f(x')} &= \frac{\tilde{x}_0^4}{4} \left(\frac{\tilde{\rho}_0^2}{f(x')} + f(x') - 2\tilde{\rho}_0 \right) = \\ & - \frac{\tilde{x}_0^4 \tilde{\rho}_0^2}{4f} + \tilde{\rho}_0 \tilde{x}_0^2 \frac{F}{f} + \frac{\tilde{x}_0^4}{4} f, \end{aligned} \quad (\text{B.7})$$

$$1 = - \frac{2}{\tilde{x}_0^2} \frac{F(x')}{f(x')} + \frac{\tilde{\rho}_0}{f(x')}. \quad (\text{B.8})$$

A solution of Eq. (B.5) can thus be found if the time dependent coefficient of the three independent spatial functions are all zero, which yields

$$\tilde{C} = \tilde{A} (\tilde{x}_0^2 b_2^0)^2 / 8, \quad (\text{B.9})$$

$$\begin{aligned} & \frac{d}{d\tau} (a\tilde{P}_c - \frac{1}{2}ab_3^2) + \frac{\dot{a}}{a} (a\tilde{P}_c - \frac{1}{2}ab_3^2) + \\ & \tilde{A} \left(a\tilde{P}_c - \frac{1}{2}ab_3^2 + \frac{(\tilde{x}_0^2 \tilde{\rho}_0 b_2^0)^2}{8a} \right) = \tilde{\Gamma} \tilde{\rho}_0, \end{aligned} \quad (\text{B.10})$$

$$\frac{d}{d\tau} (\ddot{a}a + b_2^0 b_3) + \frac{\dot{a}}{a} (\ddot{a}a + b_2^0 b_3) + \tilde{A} \left(\ddot{a}a + b_2^0 b_3 + \frac{\tilde{x}_0^2 \tilde{\rho}_0 (b_2^0)^2}{2a} \right) = 2 \frac{\tilde{\Gamma}}{\tilde{x}_0^2}. \quad (\text{B.11})$$

With Eq. (A.22)

$$\begin{aligned} b_3(\tau) &= \frac{b_3^0}{a} + \frac{b_2^0 (b_1^0)^2}{a} \int_0^\tau \int_0^{\tau'} \frac{1}{a(\tau'')} d\tau'' d\tau' \\ & \quad + b_1^0 c^0 \frac{\tau}{a}, \end{aligned} \quad (\text{B.12})$$

one obtains two time differential equations describing the whole system. These self-similar solutions are exact and no approximation is assumed but for the thermal function. Eq. (B.11) describes the evolution of a gaussian perturbation associated to an homologous velocity field, it does not depend on the central pressure. Eq. (B.10) describes the evolution of the central pressure. It depends on the evolution of the perturbation. Eq. (B.11) allows to study, at least numerically, the threshold dependence with initial velocity ($\dot{a}(0)$) and magnetic field (b_1^0 and b_3^0). This will be considered in a forthcoming study.

Appendix C: exact solution of a magnetically assisted thermal condensation

In this appendix, we find an exact solution of the idealised limit of Eq. (1-6) with the magnetic field equal to zero at the origin ($x = 0$). In this situation the magnetic pressure compresses the gas and enhances the condensation process. We start as in Appendix A and consider Eq. (A.5) with a magnetic field equal to

$$\tilde{B}_y(x', \tau) = B_2(\tau) \sqrt{H \pm F(x')}, \quad (\text{C.1})$$

where H is a constant. The evolution of \tilde{V}_y is given by the y -component of Eq. (2) that can be rewritten with Eq. (C.1)

$$\partial_\tau \tilde{V}_y + \frac{\dot{a}}{a} \tilde{x} \partial_{\tilde{x}} \tilde{V}_y = b_1^0 B_2(\tau) \frac{\pm F'(x')}{2f(x') \sqrt{H \pm F(x')}}.$$

This leads to: $\tilde{V}_y(\tau, x') = c(\tau)N(x')$, with

$$N(x') = \frac{\pm x'}{2\sqrt{H \pm F(x')}}}, \quad (\text{C.2})$$

and

$$\dot{c} = b_1^0 B_2. \quad (\text{C.3})$$

The evolution of \tilde{B}_y is given by Eq. (5) which leads to

$$\left(\dot{B}_2 + \frac{\dot{a}}{a} B_2 \right) \sqrt{H \pm F(x')} - B_1^0 \frac{c}{a} \frac{dN}{dx'}(x') = 0. \quad (\text{C.4})$$

The condition for the existence of a self-similar solution is that

$$R_0 \sqrt{H \pm F(x')} = \frac{dN}{dx'}, \quad (\text{C.5})$$

where R_0 is a constant. This leads to:

$$R_0 x' = \pm \frac{1}{4} \frac{d}{dx'} \left(\frac{x'}{\sqrt{H \pm F(x')}} \right)^2, \quad (\text{C.6})$$

and

$$H \pm F(x') = \frac{(x')^2}{cst + 2R_0(x')^2}. \quad (\text{C.7})$$

But, $F(0) = 0$, so H is equal to zero and the sign is $+$. One has:

$$\tilde{B}_y(x', \tau) = B_2(\tau) \sqrt{\frac{(x')^2}{cst + 2R_0(x')^2}}, \quad (\text{C.8})$$

where cst is a constant coming from the integration, and

$$f(x') = \frac{2cst}{cst + 2R_0(x')^2}. \quad (\text{C.9})$$

The density is a decreasing function, and the magnetic pressure an increasing function, so that magnetic pressure enhances the condensation. The time dependent functions obey the following relations

$$\dot{c} = b_1^0 B_2, \quad (\text{C.10})$$

$$\dot{B}_2 - R_0 b_1^0 \frac{c}{a} + \frac{\dot{a}}{a} B_2 = 0, \quad (\text{C.11})$$

$$(\ddot{a} + (B_2)^2) a^\gamma = K_0 \exp(-\tilde{A}\tau). \quad (\text{C.12})$$

References

- Balbus S., 1986, ApJ 304, 787
 Ballesteros-Paredes J., Vázquez-Semadeni E., Scalo J., 1999, ApJ 515, 286
 Barenblatt G.I., Zeldovich Y.B., 1972, Ann. Rev. Fluid Mech. 4, 285
 Bergeron J., Souffrin S., 1971, A&A 11, 40
 Bouquet S., Feix M.R., Fijalkow E., 1985, ApJ 293, 494
 Burkert A., Lin D.N., 2000, ApJ (in press), astro-ph/0002106
 Crutcher R.M., 1999, ApJ 520, 706
 Dalgarno A., McCray R., 1972, ARA&A 10, 375
 David L.P., Bregman J.N., 1989, ApJ 337, 97
 Dickey J.M., Lockman F.L., 1990, ARA&A 28, 215
 Elmegreen B., 1997, ApJ 480, 674
 Ferrara A., Shchekinov Yu., 1993, ApJ 417, 595
 Ferrara A., Shchekinov Yu., 1996, Geophys. Astrophys. Fluid Dynamics 84, 274
 Field G., 1965, ApJ 142, 531
 Field G., Goldsmith D., Habing H., 1969, ApJ 155, L149
 Friaça A.C.S., Jafelice L.C., 1999, MNRAS 302, 491
 Gammie C.F., Ostriker E.C., 1996, ApJ 466, 814
 Gazol-Patiño A., Passot T., 1999, ApJ 518, 748
 Hartmann D., 1994, PhD dissertation, Sterrewacht Leiden *The Leiden/Dwingeloo survey of galactic neutral hydrogen*
 Heiles C., 1987, in: Hollenbach D., Thronson H. (eds.), *Interstellar processes*, Reidel
 Hennebelle P., Pérault M., 1999, A&A 351, 309
 Joncas G., Boulanger F., Dewdney P.E., 1992, ApJ 397, 165
 Korpi M.J., Brandenburg A., Shukurov A., et al. 1999, ApJ 514, L99
 Kovalenko I.G., Shchekinov Y.A., 1999, Phys. Plasmas 6, 335
 Kulkarni S.R., Heiles C., 1987, in: Hollenbach D., Thronson H. (eds.), *Interstellar processes*, Reidel
 Lang K., 1974, *Astrophysical Formulae*, Springer-Verlag
 Li Z.Y., Shu F.H., 1997, ApJ 475, 237
 Lioure A., 1991, *L'instabilité thermique et son rôle dans la morphologie et la dynamique du milieu interstellaire*, PhD Dissertation, Université de Paris
 Loewenstein M., 1990, ApJ 349, 471
 Mac Low M.-M., McKee C.F., Klein R.I., Stone J.M., Norman M.L., 1994, ApJ 433, 757
 Miniati F., Ryu D., Ferrara A., Jones T.W., 1999, ApJ 510, 726
 Mouschovias T.C., 1976a, ApJ 206, 753
 Mouschovias T.C., 1976b, ApJ 207, 141
 Munier A., Feix M.R., 1982, ApJ 267, 344

Myers P.C., Goodman A.A., Gusten R., et al., 1995, ApJ 442, 177
Oran E.S., Mariska J.T., Boris J.P., 1982, ApJ 254, 349
Passot T., Vázquez-Semadeni E., Pouquet A., 1995, ApJ 455, 536
Ricotti M., Ferrara A., Miniati F., 1997, ApJ 485, 254
Scott E.H., Black D.C., 1980, ApJ 239, 166
Sedov L.I., 1959, *Similarity and Dimensional Methods in Mechanics*
(4th ed.), London: Infosearch

Shu F.H., 1977, ApJ 214, 488
Spitzer L., 1962, *Physics of Fully Ionised Gases* (2d ed.). New York:
Interscience
Steele C.D.C., Ibáñez M., 1999 Phys. Plasmas 6, 3086
Troland T.H., Heiles C., 1986, ApJ 301, 339
Vázquez E., Gazol A., Scalo J., 2000, ApJ (in press), astro-ph/0001027
Wolfire M.G., Hollenbach D., McKee C.F., 1995, ApJ 152, 168